metals

MDPI

Article

Gradient Recrystallization Behavior of a Moderate Warm-Rolled Non-Oriented Fe-6.5wt%Si Alloy

Haijie Xu [1,*], Cheng Xu [1], Lulan Jiang [1], Yuanxiang Zhang [2], Xuedao Shu [1] and Xiaogang Lin [3]

[1] Zhejiang Provincial Key Laboratory of Part Rolling Technology, Faculty of Mechanical Engineering and Mechanics, Ningbo University, Ningbo 315211, China
[2] The State Key Laboratory of Rolling and Automation, Northeastern University, Shenyang 110819, China
[3] Sino-Engine Technologies Co., Ltd., Ningbo 315000, China
* Correspondence: xuhaijie@nbu.edu.cn

Abstract: In Fe-Si alloy systems, the Fe-6.5wt%Si alloy shows low iron core losses and near-zero magnetostriction, thus having great potential for high-frequency applications. In this study, an Fe-6.5wt%Si alloy hot band was subjected to a moderate warm rolling with a thickness reduction of 40%, and then annealed at different temperatures. The recrystallization behavior was investigated using the EBSD technique. After the moderate warm rolling, the initial gradient structure of the hot band is inherited, leading to gradient recrystallization behaviors during the further annealing process. The sheet surface first densely nucleates and forms strong <110>//ND and {221}<114> textures. However, the <110>//ND and {221}<114> grains have fewer high-mobility and high-energy (20–45°) boundaries than the other oriented matrix grains, leading to insufficient growth advantages. In the center region, the recrystallization is slow, but the nuclei usually have larger sizes. The inheritance of the <001>//ND (θ-fiber) texture from the initial hot band appears. Some θ-fiber grains, which have easy-magnetized <001> axes lying in the sheet plane, preferentially nucleate in the strong α-fiber textured matrices and form a strong θ-fiber recrystallization texture in the center region.

Keywords: non-oriented Fe-6.5wt%Si alloy; moderate warm rolling; gradient recrystallization; nucleation; grain growth

check for updates

Citation: Xu, H.; Xu, C.; Jiang, L.; Zhang, Y.; Shu, X.; Lin, X. Gradient Recrystallization Behavior of a Moderate Warm-Rolled Non-Oriented Fe-6.5wt%Si Alloy. *Metals* **2023**, *13*, 370. https://doi.org/10.3390/met13020370

Academic Editor: Håkan Hallberg

Received: 16 December 2022
Revised: 6 February 2023
Accepted: 10 February 2023
Published: 12 February 2023

Copyright: © 2023 by the authors. Licensee MDPI, Basel, Switzerland. This article is an open access article distributed under the terms and conditions of the Creative Commons Attribution (CC BY) license (https://creativecommons.org/licenses/by/4.0/).

1. Introduction

The non-oriented Fe-Si alloy is one of the key soft magnetic functional materials in the fields of power transformation and electronics, and is one of the most widely used functional materials [1–6]. In recent years, with the popularity of the concept of environmental sustainability, more stringent requirements have been put forward for the magnetic properties of non-oriented Fe-Si alloys. The fabrication of high efficiency, low core losses, and high-quality Fe-Si alloys have been paid more and more attention. At present, the Si content in the commonly used Fe-Si alloys is generally lower than 3.5 wt%. The performance of these alloys can be effectively controlled by optimizing the process parameters. However, the low Si content limits the further improvement of magnetic properties. Compared with the common Fe-Si alloy, permalloy, and amorphous alloy, the high Si content in the Fe-6.5wt%Si alloy produces its superior magnetic properties, including high permeability, low magnetic anisotropy, low iron losses, and near-zero magnetostriction [7]. The Fe-6.5wt%Si alloy is an ideal core material for high-frequency motors, choke coils, and magnetic shields, and is beneficial for realizing the miniaturization and high efficiency of power equipment. Toyota has successfully applied the Fe-6.5wt%Si alloy to the high-frequency (15 kHz) boost converter of PRIUS hybrid vehicles [8]. Magnetics manufactures XFlux inductors and choke coils (1–20 kHz) with the Fe-6.5wt%Si alloy as the core material, mainly used as the core components of renewable energy inverters and uninterruptible power supplies [9]. DMEGC magnetics has successfully applied Fe-6.5wt%Si alloy productions to online filters and

pulse transformers [10]. These illustrated market applications show that the Fe-6.5wt%Si alloy has broad commercial prospects.

In addition to optimizing the magnetic property parameters, the high Si content in the Fe-6.5wt%Si alloy induces a solid solution strengthening effect and the appearance of ordered phases of B_2 and $D0_3$, which deteriorate its formability during deformation [11–13]. At present, some untraditional forming methods, such as chemical vapor deposition [14], spray forming [12], additive manufacturing [15], and warm rolling [16] are utilized to process Fe-6.5wt%Si alloy sheets. Among them, warm rolling is an effective method to fabricate thin sheets and adjust the microstructure evolution behaviors. Different from the common cold rolling of the Fe-3.5wt%Si alloy, the warm deformation of the Fe-6.5wt%Si alloy at 150–700 °C can decrease the ordering degree and activate a large number of slip systems, thus improving its workability. As reported by a previous study, a high Si content and warm rolling can increase the activation trend of {112}<111> slip systems in a Fe-6.5wt%Si alloy [17]. On the other hand, changing the thickness reduction rate also affects the grain rotation during warm rolling, thus resulting in various recrystallization behaviors during annealing. A number of studies have been carried out to study the evolution of the microstructure and texture during the single-stage and multi-stage warm rolling of the Fe-6.5wt%Si alloy. As reported in our previous work [17,18], the severe deformation with a single-stage rolling reduction of ~75% resulted in strong <111>//ND texture in final annealed sheets (γ-fiber, ND is the normal direction of rolling sheet). The crystals' hard-magnetized <111> axes of γ-fiber grains lie in the sheet plane, which show a deterioration effect on the magnetic properties in Fe-Si alloys. Several studies reported that coarsening the initial microstructure by normalizing the hot band can effectively weaken the formation of the recrystallized γ-fiber texture [18–20]. In addition, controlling moderate thickness reduction through multi-stage warm rolling is also an available method to inhibit the recrystallization of γ-fiber grains. Compared with severe deformation (more than 75% thickness reduction), the grain rotation and energy storage are limited after moderate deformation with a reduction rate of 30–60%. The γ-fiber deformed matrices, which usually provide nucleation sites for γ-fiber crystal nuclei, are less formed. The unstable <001>//ND (θ-fiber) oriented crystals with easy-magnetized <001> axes on the sheet plane and preferably nucleate during annealing. Yao et al. [21] discussed that the intermediate annealing after a moderate warm rolling weakened the dislocation concentration in the shear bands, resulting in the preferential nucleation of {001}<100> (Cube) and {110}<001> (Goss) grains. Using an Fe-6.5wt%Si alloy hot band with strong θ-fiber in the center region as the raw material, Liang et al. [22] prepared a strong Cube texture after a three-stage warm rolling. In each rolling stage, Cube crystals are preferably deflected to {001}<120> orientation, and then regenerated via recrystallization or recovery during intermediate annealing, resulting in excellent magnetic properties. In our previous work [17], the microstructure and slip behavior of an Fe-6.5wt%Si alloy under a 40% thickness reduction were studied. There were no shear bands within deformed grains, only some slip bands and deformation bands, indicating that the grain rotation under the moderate deformation was limited. Thus, it has great potential to promote the formation of strong θ-fiber texture by warm rolling at a moderate thickness reduction rate of 30–60%.

The present studies show that moderate warm rolling can indeed optimize the annealing texture of the Fe-6.5wt%Si alloy. However, these studies were focused on the texture evolution during moderate rolling and annealing in Fe-6.5wt%Si alloys. Hot bands usually have an inhomogeneous microstructure, which is caused by different heat transfer and deformation mechanisms from the surface to center regions. The evolution of the gradient microstructure across the thickness during warm rolling and annealing was rarely investigated in previous works. In this study, an Fe-6.5wt%Si alloy hot band with a gradient structure was subjected to moderate warm rolling. The different recrystallization behaviors in the surface region and center region were investigated, respectively.

2. Materials and Experimental Procedure

The chemical composition of the raw, non-oriented Fe-6.5wt%Si alloy in weight percent is 0.009% C, 6.5% Si, 0.011% Mn, 0.005% Al, 0.005% S. After melting the initial materials in a vacuum induction furnace, an Fe-6.5wt%Si alloy ingot was obtained. The ingot was subsequently homogenized at 1200 °C for 2 h and forged into a square billet with a thickness of 70 mm. After reheating for 30 min at 1200 °C, the billet was hot rolled to 2 mm in thickness. As shown in Figure 1, a sample with the size of 85 mm in length and 75 mm in width was cut from the hot band, which was subjected to a moderate deformation via warm rolling. The detailed rolling route has been shown elsewhere [17]. Before warm rolling, the hot band sample was heated to 650 °C and held for 3 min. During warm rolling, the sample thickness was reduced by 0.05–0.1 mm in each pass. Between each pass, the rolled sample was reheated to 650 °C for 1 min to maintain the plastic deformation ability of the Fe-6.5wt%Si alloy. After warm rolling, the initial hot band sample was rolled to a thickness of 1.2 mm. The total thickness reduction rate is 40%, and the ratio (*l*/*h*) of the length of deformation zone (*l*) to the final thickness (*h*) is 6.5. Five small specimens with the size of 10 mm × 8 mm (length × width) were cut from the warm-rolled sheet and applied to different annealing treatments. Two specimens were annealed at 750 °C for 10 min and 20 min, two specimens were annealed at 800 °C for 10 min and 20 min, and a specimen was annealed at 850 °C for 20 min.

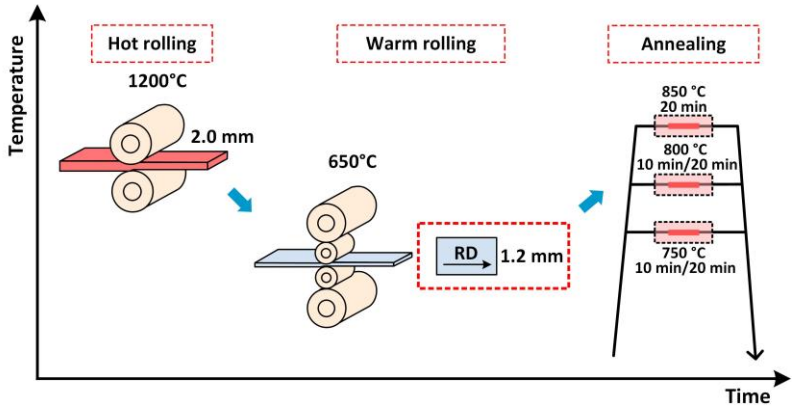


Figure 1. Schematic illustration of the hot rolling, warm rolling, and annealing processes.

The RD–ND sections (RD is rolling direction and ND is the normal direction of the sheet plane) of the annealed specimens were scanned using an electron backscatter diffraction (EBSD) technique to study the evolution of the microstructure and texture. Before the EBSD scans, the specimens were cold mounted and polished to a scratch-free state, and then polished using a 50-nm-sized colloidal silica suspension for 40 min to remove the stress layer and corrode the microstructure. An EBSD analysis was performed on a scanning electron microscopy (SEM, Zeiss Gemini 300) with scanning steps of 1.5–2.5 μm. The two-dimensional scanning area of each annealed sample was 1500 μm × 1200 μm (length × height). The orientation distribution functions (ODFs) were calculated from the measured Euler angles (Bunge notation) using a harmonic series expansion method with a maximum series rank of 22. A deviation of 15° was allowed when calculating the unique texture fibers and grain orientations.

3. Results and Discussion

3.1. Microstructure and Texture after Hot Rolling and Warm Rolling

The initial hot band shows a gradient structure along the whole thickness, as shown in Figure 2a. The surfaces are mainly composed of fine recrystallized grains and some small, deformed grains, and present strong <110>//ND texture and weak <110>//TD texture (TD is the transverse direction of the sheet plane). The center region is characterized by elongated deformation grains, which exhibit strong θ-fiber, weak α-fiber (<110>//RD) and

{111}<110> textures. The gradient structure after hot rolling is attributed to the different deformation modes and heat transfer conditions in the surface and center regions [18]. After hot rolling at 1200 °C, the formation of precipitates in the non-oriented Fe-6.5wt%Si alloy is inevitable. A small amount of Mn elements may precipitate in the form of MnS particles. A similar phenomenon has been observed in our previous work [23]. After warm rolling at 650 °C with a moderate thickness reduction rate of 40%, as shown in Figure 2b, the surface grains are thinned to elongated shapes, and the unstable <110>//ND and <110>//TD textures are transformed into stable γ-fiber and α-fiber textures. In the center region, a large number of slip bands appear, but no apparent shear bands are observed. During plastic deformation, slip bands are microbands formed on the grain surface after the crystal planes slipping along slip directions. Between the slip bands and crystal matrix, the deviation angle is usually less than 5°, which is different to the shear bands [17]. Between the shear bands and crystal matrix, high-angle grain boundaries with more than 15° misorientation angle usually form, indicating that the deformation is significantly heterogeneous. Thus, the formation of dense slip bands in the rolled sample indicates that the warm rolling with a moderate thickness reduction leads to uniform plastic deformation in the center region. The initial uniformly distributed θ-fiber components, i.e., the texture components from {001}<100> (Cube) to {001}<110> (rotated Cube), aggregate to the rotated Cube texture. The α-fiber is strengthened and the maximum density is located at the {112}<110> component. It is seen that the texture densities of the surface and center regions are apparently increased after moderate rolling. Such texture evolution is consistent with the typical rotation behaviors of different crystallographic orientations during rolling deformation [11], i.e., the unstable <110>//ND texture tends to rotate to the γ-fiber texture, the dispersed θ-fiber components prefer to concentrate at the metastable rotated Cube component, and partial rotated Cube texture can move to the {112}<110> component.

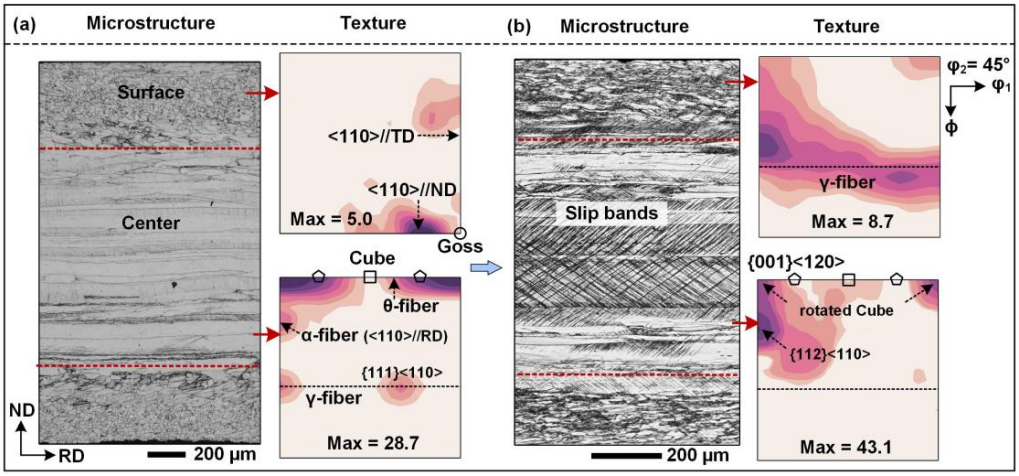


Figure 2. Microstructure and texture after hot rolling and warm rolling: (**a**) initial hot band, (**b**) the sheet after warm rolling at 650 °C with a thickness reduction of 40%.

3.2. Microstructure and Texture after Annealing at Different Temperatures

Figure 3 shows the microstructures and textures after annealing at 750 °C, 800 °C, and 850 °C for different times. As the annealing temperature increases, the gradient structure is gradually weakened, and the recrystallization fraction is increased from 47% to 100%. The fine and equiaxed grains at the surfaces grow into large sizes, and the elongated grains in the center region gradually recrystallized. After annealing at 750 °C for 10 min and 20 min, a texture inheritance phenomenon occurs at the surface regions. The initial hot rolling textures of the {221}<114> component and <110>//ND fiber, especially the Goss component, reappear through recrystallization. In the center region, a few θ-fiber grains nucleated at the boundaries of deformed matrices, resulting in the weakening of the α-fiber texture and the strengthening of the rotated Cube texture. As the annealing temperature

increases to 800 °C, almost complete recrystallization occurs. The surface grains have inhomogeneous growth rates. Some α-fiber grains abnormally grow into large sizes, while <110>//ND and {221}<114> oriented grains lack growth advantages and are consumed by neighboring grains. As a result, a strong α-fiber texture evolves at the sample surface. In the center region, the nucleated θ-fiber grains have significantly larger sizes than the surface grains, and preferably grow along the elongation direction of the deformed grains. Further increasing the annealing temperature to 850 °C, the recrystallized microstructure is similar to that after annealing at 800 °C. On the other hand, with the increase in the annealing temperature, the gradient recrystallization behavior, i.e., the rapid nucleation at sample surfaces and the slow nucleation in the center region, becomes less obvious.

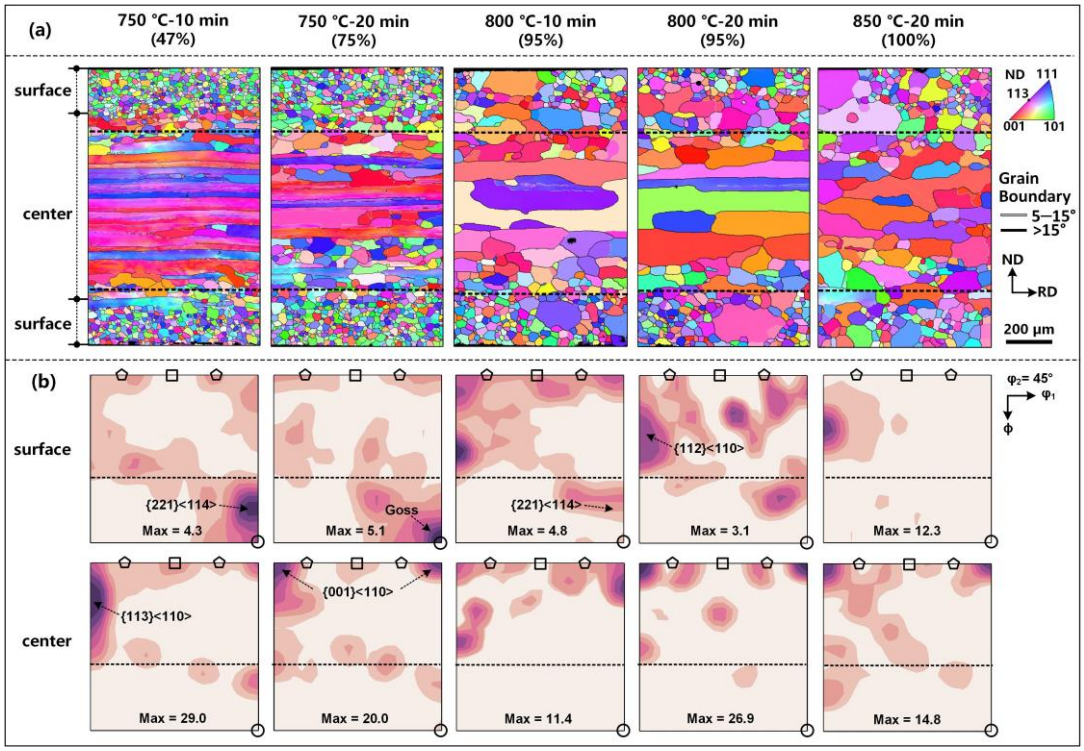


Figure 3. The microstructure and texture of Fe-6.5wt%Si alloy after annealing at different temperatures: (**a**) EBSD inverse pole figure (IPF) maps showing increasing recrystallization fraction; (**b**) the corresponding gradient textures in the surfaces and center regions respectively ($\varphi_2 = 45°$ ODF sections in Euler space using Bunge notation).

3.3. Gradient Recrystallization Behavior of the Moderate Warm-Rolled Sheets

A recrystallization process includes nucleation and grain growth. At the early stage of recrystallization, both nucleation and grain growth occur. When the deformed structure is completely consumed by new grains, the microstructure is called complete recrystallization. After this stage, the recrystallization process is dominated by grain growth behavior. During the gradient recrystallization process of the warm-rolled Fe-6.5wt%Si alloy, the preferentially nucleated <110>//ND and {221}<114> oriented grains at the surface region lack growing tendency, which is closely related to the poor boundary migration velocities. It is reported that the further grain growth after complete recrystallization is mainly driven by reducing the energy stored at the grain boundaries [24]. In the studies of grain growth mechanism after complete recrystallization, experimental results demonstrated that the grain boundaries with high mobility and high energy are easy to migrate, thus promoting grain growth [25,26]. According to the theory of grain boundary mobility proposed by Sandstrom [27] and the theory of grain boundary energy put forward by Read and Shockley [28], the variation trends of grain boundary mobility and energy with respect to the misorientation angle have been calculated in our previous work [29]. As

the misorientation angle increases, both the grain boundary migration and energy exhibit the characteristics of normal distribution. The grain boundaries with the misorientation angles between 20° and 45° have high mobility and high energy. Figure 4 shows the fraction variation of the surface grain boundary with respect to the misorientation angle in the samples annealed at 750 °C for 10 min and 20 min. It is seen that the preferentially nucleated grains, i.e., the <110>//ND and {221}<114> grains, have a much higher fraction of low-mobility and low-energy 5–20° grain boundaries, while showing less 20–45° grain boundaries (especially the 30–45° grain boundaries). In contrast, the boundaries between the preferentially nucleated grains and the matrix grains, as well as the boundaries between other matrix grains, show a higher fraction of 20–45° grain boundaries. Therefore, the high fraction of low-mobility and low-energy boundaries between the <110>//ND and {221}<114> grains gives rise to slow grain growth rates. The neighboring matrix grains grow rapidly and form size dominance, which will consume the <110>//ND and {221}<114> grains with small sizes.

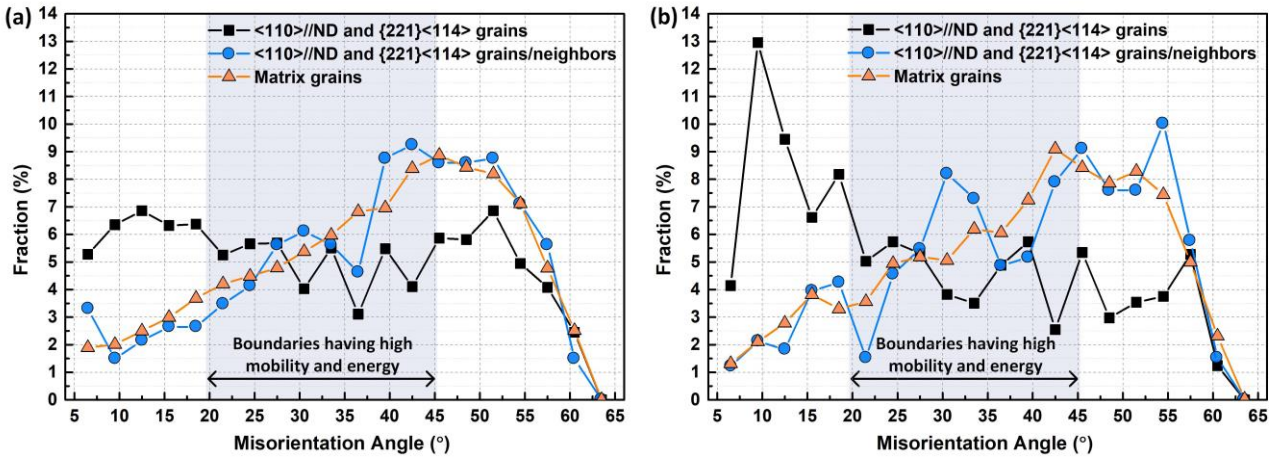


Figure 4. Misorientation angles of the grain boundaries between the preferentially nucleated grains (<110>//ND and {221}<114> grains); between the preferentially nucleated grains and neighboring grains; between matrix grains in the samples annealed at 750 °C for (**a**) 10 min and (**b**) 20 min.

Figure 5 calculates the microtextures of the surface grains in different size ranges after annealing at different temperatures. The number of small surface grains (i.e., grain sizes less than 25 μm or 35 μm) exceeds 500, and the number of other large surface grains exceeds 200, which are sufficient for the corresponding texture characterization. It is seen that after annealing at 750 °C, the grains smaller than 25 μm and the grains larger than 25 μm both show strong <110>//ND and {221}<114> textures. As grains grow, i.e., increasing the annealing temperature to 800 °C and 850 °C, the <110>//ND and {221}<114> textures in the surface grains larger than 35 μm are greatly weakened. A strong α-fiber texture dominates the microstructure, with the {112}<110> component being the sharpest. This indicates that the nucleated α-fiber grains at the surface regions have growth advantage during grain growth, thus resulting in a strong α-fiber texture.

As seen in the gradient recrystallization process, the surface region is first to recrystallize to fine and equiaxed grains, and the grains with different orientations reveal different growth rates. Differently, the center region shows slow recrystallization and discrete nucleation. Due to the limited thickness reduction after a moderate warm rolling, γ-fiber deformed grains are rarely observed, and shear banding structures in the typical, severely deformed grains have not appeared. Only numerous net-shaped distributed slip bands are formed, leading to homogenous strain distribution in deformed grains. Figure 6 shows the recrystallization behavior in the center regions of the moderate warm-rolled sheets. It is seen that the nucleated grains have Cube, {001}<120>, rotated Cube, {114}<481> and {112}<110> orientations.

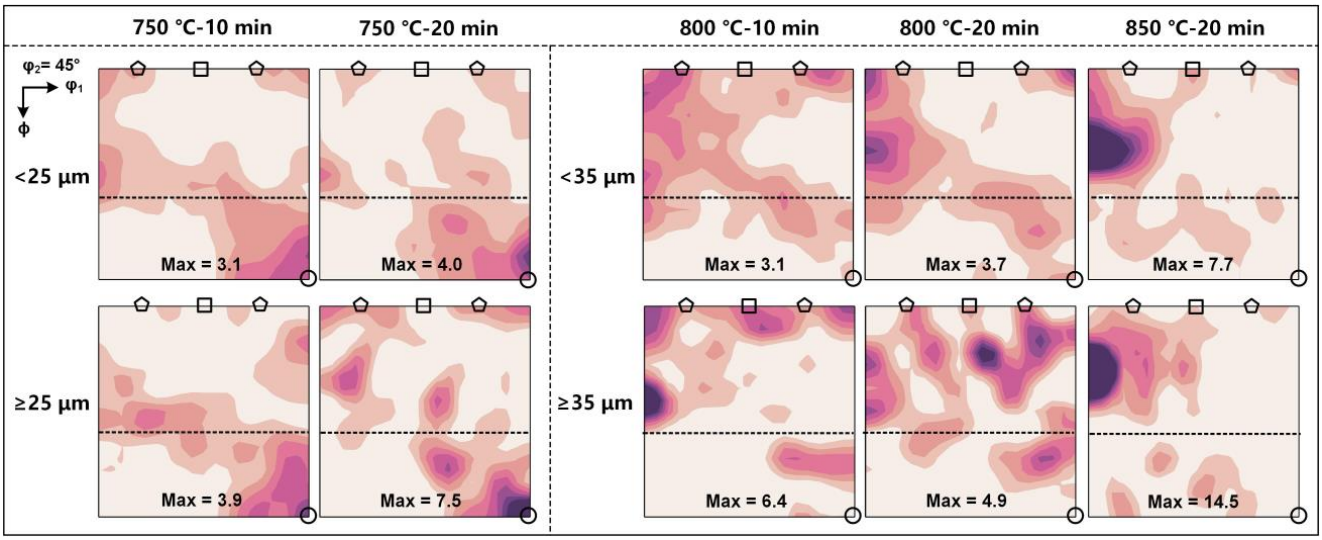


Figure 5. The texture evolution of the surface recrystallized grains in different grain-size ranges after annealing at different temperatures (φ_2 = 45° ODF sections).

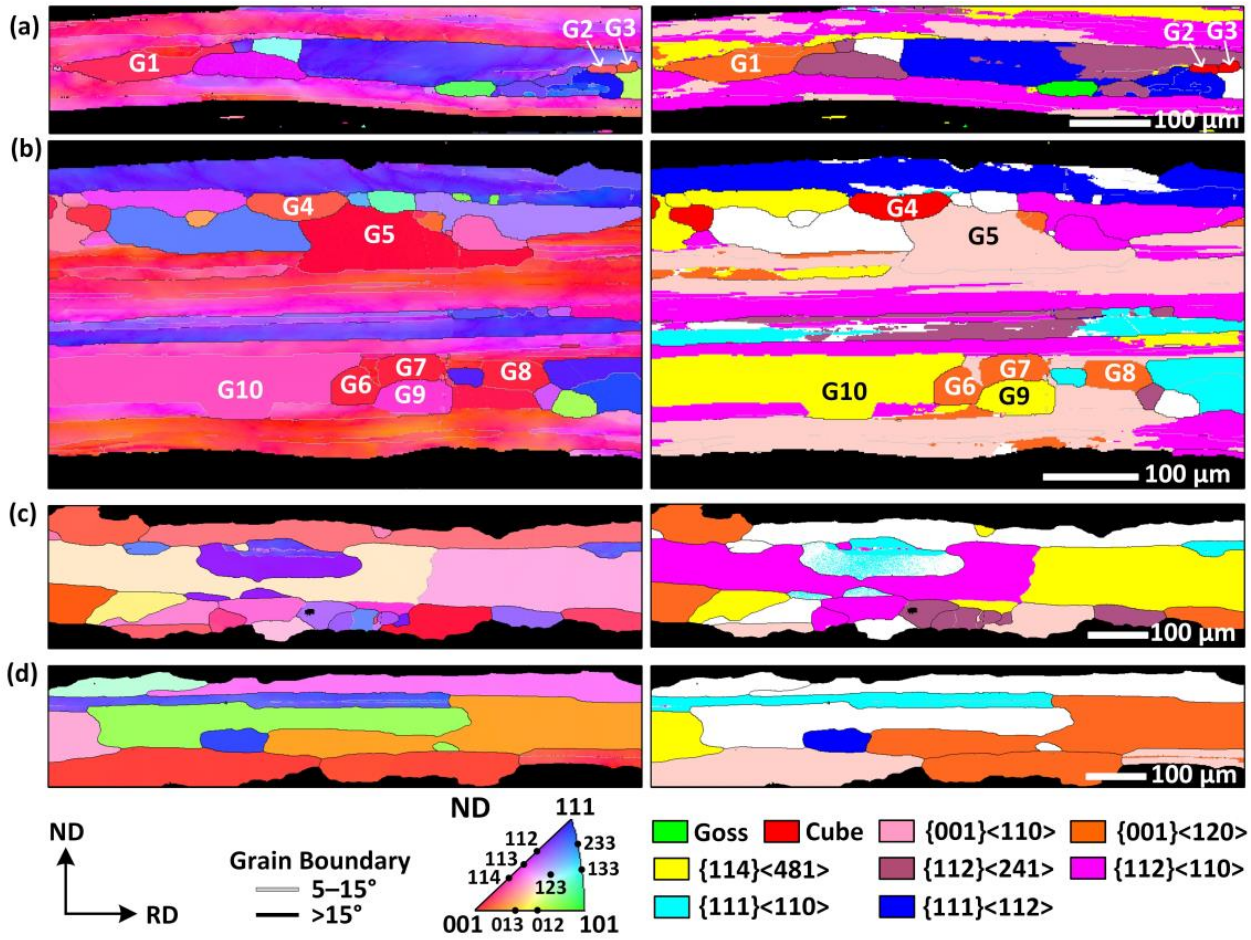


Figure 6. The recrystallization behaviors of the center region after annealing at 750 °C for (**a**) 10 min and (**b**) 20 min, and annealing at 800 °C for (**c**) 10 min and (**d**) 20 min. The IPF maps are on the left and the grain unique color maps are on the right.

The Cube grains marked as G2, G3, and G4, mainly nucleate at the prior boundaries between the {111}<112> and {112}<241> deformed matrices, and between the {111}<112>

and {001}<120> matrices. The possible origins of recrystallized Cube grains were also reported by other studies. Jiao et al. [30] pointed out Cube grains nucleated in the retained Cube-oriented deformation bands in a cold-rolled Fe-6.5wt%Si alloy. Takajo et al. [31] reported that Cube grains nucleated in {114}<481> deformed grains and showed growth advantage using an in situ EBSD technique. Mehdi et al. [32] observed low stored energy Cube crystallites within the shear bands of the {110}<110> matrix, which served as the initial Cube seeds for nucleation. Park et al. [33] reported that Cube grains nucleated in the shear bands of {111}<112> deformed grains and formed within {112}<110> deformed grains. However, these mechanisms were not observed in the annealed samples. The moderate deformation results in the absence of shear bands and a small amount of Cube nucleation. The nucleation of {001}<120> grains is highly related to the α-fiber-deformed grains, and tends to form low-angle grain boundaries with the 5–15° misorientation. As shown in Figure 6a, the {001}<120> grain G1 nucleates in a {112}<110> deformed grain, and is neighboring to the {114}<481> oriented matrix region. This similar nucleation phenomenon also has been reported in our previous study [18]. In addition, as shown in Figure 6b, the {001}<120> grains G6, G7, and G8 nucleate in a rotated Cube-deformed grain, and have small deviation angles of 6.3–10.5° to the neighboring matrices. Similar with {001}<120> nucleation, a rotated Cube grain G5 nucleates in the rotated Cube-deformed matrix and grow into a large size. The misorientation between the rotated Cube nucleation G5 and the matrix is 11.3°.

Besides these favorable θ-fiber recrystallized grains, some {114}<481> grains, such as grains G9 and G10, also appear during annealing. The {114}<481> grain G9 originates in a rotated Cube grain and nucleates beside the two {001}<120> grains G6 and G7. The {114}<481> grain G10 nucleates at the front boundary of a {112}<110> deformed grain and grows into a significantly large size along the elongation direction of the deformed matrix. The {114}<481> texture is a typical α*-fiber ({11 h}<1 2 1/h>) component in an Fe-Si alloy, which is generally accepted to originate in α-fiber-deformed grains [18,34,35]. Zhang et al. [34] found that α*-fiber grains in a Fe-3.0wt%Si alloy nucleated in the α-fiber grains with rotated Cube-{112}<110> orientations and showed growth advantages. As reported by Gobernado, the {113}<361> deformation bands were formed by the fragmentation of the rotated Cube grains during the cold rolling of IF steel, which recrystallized into {113}<361> grains [36]. The {113}<361> texture is only of a ~6° deviation to the {114}<481> texture. As the recrystallization gradually completes, as shown in Figure 6c and 6d, the Cube grains disappear, while the grains with {001}<112>, rotated Cube, and {114}<481> orientations survive and evolve into larger sizes. Therefore, the warm rolling deformation with a moderate thickness reduction is beneficial to promote the formation of a favorable θ-fiber texture in the central region during recrystallization.

From the above analysis, it is seen that the recrystallization of a moderate warm-rolled Fe-6.5wt%Si alloy shows different behaviors from the heavily rolled Fe-Si alloys. The limited reduction rate preserves the gradient structure of the initial hot-rolled microstructure, i.e., the surfaces are composed of fine deformed grains and the center region has coarse and elongated grains. During annealing, the surface layers first complete recrystallization, and form a fine and homogenous microstructure. Owing to the high fraction of low-mobility and low-energy 5–20° boundaries between the initially strong textured <110>//ND and {221}<114> grains, they are gradually invaded by the neighboring α-fiber grains with growth advantages, resulting in a strong {112}<110> texture at the surface regions. In the center regions, due to the moderate thickness reduction, strain distribution in the deformed grains is uniform. No shear bands evolve, which commonly provide nucleation sites for the recrystallized grains that have significantly different orientations from the matrices. Thus, the recrystallization process of center region is dominated by scattered nucleation and further grain growth along the elongated matrices. The α-fiber deformed matrices, i.e., the {001}<110> and {112}<110> oriented grains, facilitate the recrystallization of the Cube, rotated Cube, and the {001}<120> and {114}<481> grains, leading to a strong θ-fiber texture and a soft α*-fiber texture. This final recrystallized texture of the center region is very

similar to that of the initial hot band texture. This indicates that warm rolling at a moderate thickness reduction of 40% can induce texture inheritance of the favorable θ-fiber texture. Therefore, introducing a moderate warm rolling into the preparation of Fe-6.5wt%Si alloy sheets is expected to improve the magnetic properties.

4. Conclusions

An Fe-6.5wt%Si alloy hot band was processed by warm rolling at a moderate thickness reduction of 40%. The recrystallization behavior during annealing at different temperatures was studied using the EBSD method. The main findings can be summarized as follows.

(1) The initial gradient structure of the hot band is inherited after warm rolling with a moderate thickness reduction of 40%, i.e., the surface regions are composed of fine deformed grains with strong α-fiber and γ-fiber textures, and the center region consist of coarse and elongated grains with strong α-fiber and θ-fiber textures.
(2) During the annealing process of the moderate warm-rolled sheet, a gradient recrystallization phenomenon along the thickness occurs. The surface first densely nucleates and completely recrystallizes into fine equiaxed grains with strong <110>//ND and {221}<114> textures. The center region shows slower recrystallization. The absence of shear bands results in fewer nucleated grains, but larger grain sizes after growth.
(3) During grain growth at the surface regions, the boundaries between the <110>//ND and {221}<114> grains have a small fraction of high-mobility and high-energy 20–45° boundaries than those between other oriented matrix grains, leading to insufficient grain growth advantage.
(4) During recrystallization of the center region, warm rolling at a moderate thickness reduction induces θ-fiber inheritance from the initial hot band. The grains with θ-fiber and {114}<481> orientations nucleate in the strong α-fiber textured and deformed matrices, and form final strong θ-fiber and soft α*-fiber textures.

Author Contributions: H.X.: Conceptualization, investigation, writing—original draft. C.X.: conceptualization, writing—review and editing. L.J.: Conceptualization, writing—review and editing. Y.Z.: Writing—review and editing, funding acquisition. X.S.: Supervision, resources, funding acquisition. X.L.: Supervision, funding acquisition. All authors have read and agreed to the published version of the manuscript.

Funding: This work was financially supported by National Natural Science Foundation of China (Grant No. 52205385). the Open Research Fund from the State Key Laboratory of Rolling and Automation, Northeastern University (Grant No. 2021RALKFKT002), Ningbo Natural Science Foundation (Grant No. 2021J098), Ningbo Science and Technology Major Project (Grant No. 2022Z055).

Institutional Review Board Statement: Not applicable.

Informed Consent Statement: Informed consent was obtained from all subjects involved in the study.

Data Availability Statement: The raw/processed data required to reproduce these findings cannot be shared at this time due to technical/time limitations.

Conflicts of Interest: There are no known competing financial interests or personal relationships that could have appeared to influence the work reported in this paper.

References

1. Gurbuz, I.; Martin, F.; Aydin, U.; Asaf, A.; Chamosa, M.; Rasilo, P.; Belahcen, A. Experimental characterization of the effect of uniaxial stress on magnetization and iron losses of electrical steel sheets cut by punching process. *J. Magn. Magn. Mater.* **2022**, *549*, 168983. [CrossRef]
2. Tamimi, S.; He, Y.; Sanjari, M.; Pirgazi, H.; Kockelmann, W.; Robinson, F.; Mohammadi, M.; Kestens, L. Mechanical properties and crystallographic texture of non-oriented electrical steel processed by repetitive bending under tension. *Mater. Sci. Eng. A* **2022**, *835*, 142665. [CrossRef]
3. Okubo, T.; Uesaka, M.; Zaizen, Y.; Oda, Y. Method of Manufacturing Non-Oriented Electrical Steel Sheet. U.S. Patent 2022010400A1, 13 January 2022.

4. Feng, F.; Che, S.; Wang, F.; Zhao, Y.; Zhang, Y.; Wang, Y.; Cao, G.; Yuan, G.; Misra, R.; Wang, G. Microstructure evolution and strengthening mechanism in thin-gauge non-oriented silicon steel with high strength. *J. Magn. Magn. Mater.* **2022**, *563*, 169791. [CrossRef]
5. He, Y.; Hilinski, E. Textures of non-oriented electrical steel sheets produced by skew cold rolling and annealing. *Metals* **2022**, *12*, 17. [CrossRef]
6. Shen, X.; Meng, F.; Lau, K.; Wang, P.; Lee, C. Texture and microstructure characterizations of Fe-3.5wt%Si soft magnetic alloy fab-ricated via laser powder bed fusion. *Mater. Charact.* **2022**, *189*, 112012. [CrossRef]
7. Ouyang, G.; Chen, X.; Liang, Y.; Macziewski, C.; Cui, J. Review of Fe-6.5 wt% Si high silicon steel-A promising soft magnetic mate-rial for sub-kHz application. *J. Magn. Magn. Mater.* **2019**, *481*, 234–250. [CrossRef]
8. You, B.; Kim, J.; Lee, B.; Choi, G.; Yoo, D. Optimization of powder core inductors of buck-boost converters for hybrid electric vehicles. In Proceedings of the 2009 IEEE Vehicle Power and Propulsion Conference, Dearborn, MI, USA, 7–11 September 2009; pp. 730–735.
9. *Magnetics XFlux® Cores*; Magnetics: Pittsburgh, PA, USA, 2016; pp. 1–4.
10. *Alloy Powder Ring Cores*; Hengdian Group Dmegc Magnetics Co., Ltd.: Dongyang, China, 2018; pp. 1–24.
11. He, Z.; Zhao, Y.; Luo, H. *Electrical Steel*; Metallurgical Industry Press: Beijing, China, 2012.
12. Cava, R.; Botta, W.; Kiminami, C.; Olzon-Dionysio, M.; Souza, S.; Jorge, A.; Bolfarini, C. Ordered phases and texture in spray-formed Fe-5wt%Si. *J. Alloys Compd.* **2011**, *509*, S260–S264. [CrossRef]
13. Rementeria, R.; Poplawsky, J.; Aranda, M.; Guo, W.; Jimenez, J.; Garcia-Mateo, C.; Caballero, F. Carbon concentration measure-ments by atom probe tomography in the ferritic phase of high-silicon steels. *Acta Mater.* **2017**, *125*, 359–368. [CrossRef]
14. Takamiya, T.; Hanazawa, K.; Suzuki, T. Recent development of grain-oriented electrical steel in JFE Steel. *JFE Tech. Rep.* **2016**, *21*, 1–6.
15. Cramer, C.; Nandwana, P.; Yan, J.; Evans, S.; Paranthaman, M. Binder jet additive manufacturing method to fabricate near net shape crack-free highly dense Fe-6.5 wt.% Si soft magnets. *Heliyon* **2019**, *5*, e02804. [CrossRef]
16. Zhang, Y.; Lu, X.; Yuan, G.; Wang, Y.; Fang, F.; Zhang, X.; Wang, G. Texture and microstructure evolution during different rolling methods in strip-cast grain-oriented 6.5% Si steel. *J. Magn. Magn. Mater.* **2020**, *499*, 166256. [CrossRef]
17. Xu, H.; Xu, Y.; He, Y.; Cheng, S.; Jiao, H.; Yue, S.; Li, J. Two-stage warm cross rolling and its effect on the microstructure, texture and magnetic properties of an Fe-6.5 wt% Si non-oriented electrical steel. *J. Mater. Sci.* **2020**, *55*, 12525–12543. [CrossRef]
18. Xu, H.; Xu, Y.; Jiao, H.; Cheng, S.; Misra, R.; Li, J. Influence of grain size and texture prior to warm rolling on microstructure, tex-ture and magnetic properties of Fe-6.5 wt% Si steel. *J. Magn. Magn. Mater.* **2018**, *453*, 236–245. [CrossRef]
19. Lee, K.; Huh, M.; Lee, H.; Park, J.; Kim, J.; Shin, E.; Engler, O. Effect of hot band grain size on development of textures and mag-netic properties in 2.0% Si non-oriented electrical steel sheet. *J. Magn. Magn. Mater.* **2015**, *396*, 53–64. [CrossRef]
20. Paolinelli, S.; Cunha, M.; Cota, A. Effect of hot band grain size on the texture evolution of 2% Si non-oriented steel during final annealing. *IEEE Trans. Magn.* **2015**, *51*, 1–4. [CrossRef]
21. Yao, Y.; Sha, Y.; Liu, J.; Zhang, F.; Zuo, L. Texture and microstructure for magnetic properties of two-stage cold-rolled Fe-6.5 wt pct Si thin sheets. *Metall. Mater. Trans. A* **2016**, *47*, 5771–5776. [CrossRef]
22. Liang, R.; Yang, P.; Mao, W. Cube texture evolution and magnetic properties of 6.5 wt% Si electrical steel fabricated by surface energy and three-stage rolling method. *J. Magn. Magn. Mater.* **2018**, *457*, 38–45. [CrossRef]
23. Xu, H. Study on Microstructure Evolution and Preferred Orientation in Warm-Rolled Fe-6.5wt%Si Steel. Ph.D. Thesis, Northeastern University, Shenyang, China, 2021.
24. Humphreys, F.; Hatherly, M. *Recrystallization and Related Annealing Phenomena*; Elsevier: Amsterdam, The Netherlands, 2012.
25. Lu, X.; Fang, F.; Zhang, Y.; Wang, Y.; Yuan, G.; Xu, Y.; Misra, R.; Zhang, W.; Wang, G. Microstructure and magnetic properties of strip-cast grain-oriented 4.5%Si steel under isochronal and isothermal secondary annealing. *J. Mater. Sci.* **2018**, *53*, 2928–2941. [CrossRef]
26. Song, H.; Wang, Y.; Esling, C.; Wang, G.; Liu, H. The role of grain colony on secondary recrystallization in grain-oriented electri-cal steel: New insights from an original tracking experiment. *Acta Mater.* **2020**, *206*, 116611. [CrossRef]
27. Sandsttrom, R. Subgrain growth occurring by boundary migration. *Acta Metall.* **1977**, *25*, 905–911. [CrossRef]
28. Read, W.; Shockley, W. Dislocation models of crystal grain boundaries. *Phys. Rev.* **1950**, *78*, 275–289. [CrossRef]
29. Xu, H.; Xu, Y.; He, Y.; Jiao, H.; Yue, S.; Li, J. A quasi in-situ EBSD study of the nucleation and growth of Goss grains during prima-ry and secondary recrystallization of a strip-cast Fe-6.5 wt% Si alloy. *J. Alloys Compd.* **2021**, *861*, 158550. [CrossRef]
30. Jiao, H.; Xu, Y.; Zhao, L.; Misra, R.; Tang, Y.; Liu, D.; Hu, Y.; Zhao, M.; Shen, M. Texture evolution in twin-roll strip cast non-oriented electrical steel with strong Cube and Goss texture. *Acta Mater.* **2020**, *199*, 311–325. [CrossRef]
31. Takajo, S.; Merriman, C.; Vogel, S.; Field, D. In-situ EBSD study on the cube texture evolution in 3 wt% Si steel complemented by ex-situ EBSD experiment-From nucleation to grain growth. *Acta Mater.* **2019**, *166*, 100–112. [CrossRef]
32. Mehdi, M.; He, Y.; Hilinski, E.; Kestens, L.; Edrisy, A. The evolution of cube ({001}<100>) texture in non-oriented electrical steel. *Acta Mater.* **2020**, *185*, 540–554.
33. Park, J.; Szpunar, J. Evolution of recrystallization texture in nonoriented electrical steels. *Acta Mater.* **2003**, *51*, 3037.e3051. [CrossRef]
34. Zhang, N.; Yang, P.; Mao, W. {001}<120>-{113}<361> recrystallization textures induced by initial {001} grains and related microstructure evolution in heavily rolled electrical steel. *Mater. Charact.* **2016**, *119*, 225–232.

35. Verbeken, K.; Kestens, L.; Nave, M. Re-evaluation of the Ibe-Lücke growth selection experiment in a Fe-Si single crystal. *Acta Mater.* **2005**, *53*, 2675–2682. [CrossRef]
36. Gobernado, P.; Petrov, R.H.; Kestens, L.A. Recrystallized {311}<136> orientation in ferrite steels. *Scr. Mater.* **2012**, *66*, 623–626.

Disclaimer/Publisher's Note: The statements, opinions and data contained in all publications are solely those of the individual author(s) and contributor(s) and not of MDPI and/or the editor(s). MDPI and/or the editor(s) disclaim responsibility for any injury to people or property resulting from any ideas, methods, instructions or products referred to in the content.